

Epigenome stability after DNA damage through conservative redistribution of parental histones coupled to repair

Salomé Adam^{1,2,4}, Juliette Dabin^{1,4}, Odile Chevallier¹, Olivier Leroy³, Olivier Renaud³, Geneviève Almouzni², Sophie Polo^{1,*}

¹ Laboratory of Epigenome Integrity, Epigenetics & Cell Fate Centre, UMR7216 CNRS, Paris Diderot University, Sorbonne Paris Cité, 75205 Paris cedex 13, France

² Laboratory of Chromatin Dynamics, UMR3664 CNRS, Institut Curie, PSL Research University, 75248 Paris cedex 5, France

³ Cell and tissue imaging facility, UMR3215/U934 PICT-IBiSA, Institut Curie, 75248 Paris cedex 5, France

⁴ Co-first author

*Correspondence: sophie.polo@univ-paris-diderot.fr (S.E.P)

SUMMARY

Chromatin integrity, although critical for cell function and identity, is challenged by DNA damage. Understanding how the original chromatin architecture and the information that it conveys are preserved after genotoxic stress is thus of fundamental importance. Here, by exploiting real-time tracking of parental and newly synthesized H3 histones after local UVC irradiation in human cells, we show that parental histones are not massively evicted from damaged chromatin and replaced by new histones, but instead are rapidly redistributed near damaged regions. Most parental histones subsequently recover and mix with new histones in repairing chromatin. Parental histone redistribution and recovery are both tightly coordinated with repair progression through the UVC damage sensor DDB2 (DNA Damage Binding protein 2). We propose that such conservative dynamics of parental histones in damaged chromatin contribute to keep a memory of the original chromatin landscape, which is key for epigenome stability in response to DNA damage.

HIGHLIGHTS

- Parental H3 histones redistribute to the vicinity of UVC-damaged regions
- Parental histone redistribution is controlled by the damage sensor DDB2
- Most parental histones recover and mix with new histones in repairing chromatin
- Recovery of parental histones is coupled to repair progression through DDB2 release

INTRODUCTION

Cellular genomes are constantly exposed to various sources of DNA damage (Ciccia and Elledge, 2010; Hoeijmakers, 2009; Jackson and Bartek, 2009), which threatens not only genome stability but also the integrity of their organization into chromatin. Chromatin basic unit is the nucleosome core particle where DNA is wrapped around an octamer of histone proteins comprising an $(H3-H4)_2$ tetramer flanked by two H2A-H2B dimers (Kornberg, 1977). Variations at the level of this repetitive unit, through histone variants and post-translational modifications (Bannister and Kouzarides, 2011; Maze et al., 2014; Talbert and Henikoff, 2010), as well as further chromatin compaction, constitute a major source of information that dictate gene expression and cell identity (Probst et al., 2009). How chromatin is reorganized in response to DNA damage while preserving the information that it carries is thus a fundamental issue.

Our current view of chromatin dynamics in response to DNA damage in human cells is based on the Access-Repair-Restore (ARR) model (Green and Almouzni, 2002; Smerdon, 1991; Soria et al., 2012). According to this model, chromatin is first disorganized in response to DNA damage, which facilitates access to repair factors, followed by restoration of chromatin structure. Because chromatin restoration involves the deposition of newly synthesized histones in response to UVC damage (Adam et al., 2013; Dinant et al., 2013; Polo et al., 2006), it was postulated that at least a subset of parental histones were evicted from chromatin during the Access step, which entails a potential loss of the original epigenetic information (Figure 1A). Additionally, recent reports provide evidence for nucleosome destabilization and histone eviction in response to UVC irradiation (Lan et al., 2012; Wang et al., 2006), and also during DNA double-strand break (DSB) repair (Goldstein et al., 2013; Xu et al., 2010). A massive loss of parental histones from damaged chromatin could be particularly detrimental for epigenome maintenance.

For understanding how chromatin integrity is preserved in response to genotoxic stress, it is thus critical to examine the fate of parental histones that were present in chromatin before damage infliction and carry the original epigenetic information. Here, we developed two complementary approaches for tracking parental histone dynamics in response to UVC damage in human cells, focusing on histone H3 variants. Challenging the existing model, for chromatin rearrangements in response to DNA damage, we show that, rather than being evicted from damaged chromatin, parental histones redistribute in a conservative manner and subsequently recover in damaged chromatin regions where they mix with newly synthesized histones. Our mechanistic studies demonstrate that both the redistribution and recovery of parental histones are tightly coordinated with repair progression through the UVC damage sensor protein DDB2. Altogether, our data strongly support a conservative model by which parental histone dynamics coupled to DNA damage repair contribute to the maintenance of epigenome integrity during the response to UVC damage.

RESULTS

Rapid mobilization of parental H3 histones from UVC-damaged chromatin regions

In order to determine the fate of pre-existing histones in damaged chromatin regions, we developed two complementary approaches combining UVC laser micro-irradiation with specific tracking of parental histones in live cells. We first took advantage of the SNAP-tag technology to fluorescently label old histones 48 h prior to irradiation (see Figure 1A & experimental procedures for details) in U2OS cells that stably express H3.3-SNAP histones (Dunleavy et al., 2011) and a GFP-tagged version of the repair factor XPC (Xeroderma Pigmentosum C) for visualizing damage sites in live cells (see Figure S1A for a characterization of the cell line). Real-time imaging of parental H3.3 dynamics after local UVC irradiation revealed a rapid reduction of the red fluorescence associated with old H3.3, which was restricted to the damaged chromatin area marked by GFP-XPC and detectable at least for 1 hour after irradiation (Figure 1B). We observed a similar decrease of parental H3.3 signal in cells that do not express GFP-XPC (Figure 1C), thus showing that exogenous expression of this repair protein does not alter the histone response to UVC laser micro-irradiation. We ruled out the possibility that the decrease in parental H3.3 signal observed at UVC damage sites could correspond to the neo-formation of a nucleolus (Figure S1B) and could result from photo-bleaching of the red fluorescence by the UVC laser, as irradiating paraformaldehyde-fixed cells with UVC did not reduce the red signal (Figure 1C). Thus, the observed decrease in old H3.3 signal in UVC-irradiated chromatin regions truly reflects enhanced dynamics of parental H3.3 histones in response to genotoxic stress. Furthermore, when we deliberately photo-bleached the red fluorescence in the absence of DNA damage by locally illuminating living cells with a 555 nm laser, we observed an immediate loss of the red signal while UVC laser micro-irradiation led to a progressive reduction of the red fluorescence, with a maximum of 40% loss 10 minutes after DNA damage infliction (Figure 1C). These features of parental H3.3 dynamics were recapitulated by labeling pre-existing histones with a green-fluorescent SNAP reagent instead of the red one (data not shown).

To ensure that SNAP-tag-based labeling did not interfere with parental H3 dynamics in response to DNA damage, we also developed a complementary strategy to track parental histones, based on photo-activation of PA-GFP (photo-activatable GFP) 48 h before UVC laser micro-irradiation in U2OS cells engineered to stably express H3.3-PA-GFP and RFP-XPC (see Figure S1C & experimental procedures for details). In line with our previous findings, we observed a marked reduction of parental H3.3 signal in UVC-damaged chromatin regions within minutes after laser micro-irradiation in live cells and not in paraformaldehyde-fixed cells (Figures S1D and S1E). Thus, regardless of the strategy used to monitor old histone dynamics, our data reveal a local loss of parental H3.3 histone signal in damaged chromatin regions.

Furthermore, the altered distribution of parental histones in response to UVC damage was observed in all irradiated cells, throughout interphase (Figure S1F), and was not restricted to the H3.3 variant as we observed that parental H3.1 signal was also reduced at UVC damage sites (Figure S1G).

Collectively, these results demonstrate that parental H3 histones are rapidly mobilized from UVC-damaged chromatin regions.

Conservative redistribution of parental histones to the vicinity of UVC-damaged regions

We next sought to characterize the local reduction in old H3 staining in response to UVC irradiation to determine if it reflects an actual loss of parental histones from damaged chromatin, causing a loss of epigenetic information. For this, we measured changes in old H3.3 fluorescence in the entire volume of the cell nucleus after local UVC damage. To be sensitive enough, we minimized the size of the area labeled with parental histones either by photo-bleaching H3.3-SNAP-associated fluorescence in most of the nucleus or by local photo-activation of H3.3-PA-GFP (see Figures 2A, S2A & experimental procedures for details). Doing so, we could detect a 20% loss of fluorescence from the entire nucleus upon photo-bleaching inside the fluorescent patch of parental H3.3-SNAP histones (Figure 2B). In contrast, targeting UVC irradiation to the fluorescent patch of parental histones, while leading to a comparable loss of signal in the irradiated area (around 40%), did not result in a detectable loss of fluorescence in the entire nucleus (Figure 2B). From these results we conclude that the parental H3 histones mobilized early after genotoxic stress remain in the damaged nucleus and are not subject to massive degradation.

We then refined our analysis by quantifying the distribution of the old H3.3 signal around the damaged area 15 minutes post local UVC irradiation (Figures 2A and 2C). Remarkably, we observed that the depletion of fluorescence in the center of the damaged region was accompanied by an enrichment in the surrounding area, which balanced the loss (Figures 2C and 2D). Importantly, this conservative redistribution of parental histones after local UVC irradiation was not observed upon local photo-bleaching of old histone fluorescence. We obtained similar results using SNAP-tag-based and photo-activation-based tracking of parental histones (Figure S2A-S2D). Such redistribution of parental histones in response to UVC irradiation argues against a model where pre-existing H3 histones would be evicted from damaged chromatin, as, if solubilized in the nucleoplasm, they would not occupy a defined zone in the vicinity of the irradiated region. Supporting this idea, detergent extraction of live cells after UVC irradiation did not alter the redistribution pattern of parental histones, indicating that these mobilized histones were still chromatin-associated (Figure S2E).

Furthermore, parental histone redistribution in response to UVC irradiation was accompanied by an expansion of the fluorescent patch of parental histones (Figure 2B and S2B). In line with this expansion, we measured around 20% loss of DNA density in UVC-damaged

chromatin regions 15 minutes after irradiation (Figure 2E, to be compared with 40% loss of old H3.3 signal).

Altogether, these data demonstrate that parental H3 histones are redistributed in a conservative-manner near the damaged area, by a process that involves damaged chromatin expansion.

The UVC damage sensor DDB2 is critical for parental histone redistribution

To characterize the molecular determinants of parental H3 redistribution to the vicinity of UVC-damaged regions, we first explored the connection with UVC damage repair. We observed a dose-dependent mobilization of parental H3.3 in UVC-damaged regions (Figure 3A), based on which we decided to analyze the impact of depleting NER factors involved at different steps of UVC damage repair (Figure 3B & S3A; reviewed in (Alekseev and Coin, 2015; Marteijn et al., 2014)). Decreasing the expression of the late repair factor XPG (Xeroderma Pigmentosum G), required for excision of the damaged oligonucleotide before repair synthesis, did not markedly impair parental H3.3 redistribution upon UVC irradiation (Figure S3B). Similarly, the early repair factor ERCC6 (Excision-Repair Cross-Complementing 6), involved in damage recognition within transcribed genes, was dispensable for parental H3.3 mobilization. Consistent with this finding, we did not notice any significant defects in old H3.3 mobilization in cells treated with a transcription inhibitor prior to UVC irradiation (data not shown). These results thus indicate that the mobilization of pre-existing H3 histones in response to DNA damage is not linked to transcription-coupled repair nor to late repair steps.

By contrast, we observed that depleting the UVC damage sensor DDB2 (DNA Damage Binding protein 2), involved in global genome repair, strikingly reduced old H3.3 mobilization in response to DNA damage (Figure 3C). Similar phenotypes were observed whether the knocked-down cells express or not a tagged version of XPC (data not shown), thus ruling out the possibility that exogenous expression of this repair factor could perturb the NER-coupled dynamics of parental histones. We also confirmed the requirement for DDB2 in this response by transfecting cells with a second siRNA, targeting a distinct region in DDB2 mRNA (Figure S3C). However, we did not observe a marked defect in parental H3 mobilization in response to UVC irradiation upon down-regulation of the DDB2 partners, DDB1 and CUL4A (Cullin 4A) (Figure 3C), which altogether are part of an E3-ubiquitin ligase complex that modifies various substrates at sites of UVC damage ((Nouspikel, 2011), Figure 3B). Consistent with the minor impact of depleting DDB1 and CUL4A on parental H3 mobilization, preventing *de novo* ubiquitylation reactions taking place at damage sites by treating cells with a proteasome inhibitor did not markedly alter the redistribution of old H3.3 in damaged chromatin regions (Figure S3D). These data thus demonstrate that the ubiquitylation activity of the DDB1-DDB2-CUL4A containing complex does not play a

major role in parental histone mobilization in response to UVC damage. Parental H3 redistribution to the vicinity of damaged chromatin regions is thus coupled to the earliest steps of global genome NER, with a prominent role for DDB2.

To further characterize the contribution of DDB2 to old histone redistribution upon UVC irradiation, we tested the effect of DDB2 over-expression as opposed to its down-regulation. We observed that expressing an exogenous form of DDB2 significantly increased the area of parental histone redistribution in the vicinity of UVC-irradiated regions 15 minutes after local UVC irradiation: this area was 50% larger in cells expressing GFP-DDB2 than in cells expressing GFP-XPC (Figure 3D). These results thus indicate that DDB2 is limiting for parental histone mobilization in UVC-irradiated chromatin regions. Furthermore, artificial tethering of DDB2 to a LacO (Lactose Operator) array in the absence of DNA damage in U2OS cells stably expressing H3.3-SNAP histones led to a marked reduction of parental H3.3 histone density in the LacO array (Figure 3E). These results reveal that DDB2 tethering to chromatin is sufficient for parental histone mobilization in the absence of DNA damage. Collectively, our data put forward the early repair factor DDB2 as a master regulator of parental H3 redistribution in the vicinity of UVC sites as DDB2 is necessary, limiting and sufficient for this process.

Parental H3.3 redistribution is independent of new H3.3 deposition

As we demonstrated in a previous study that the early repair factor DDB2 also controls the recruitment of the histone chaperone HIRA, which promotes the deposition of newly synthesized histones H3.3 at UVC damage sites (Adam et al., 2013), we decided to investigate the potential coupling between parental and new H3.3 dynamics in response to UVC irradiation. For this, we first characterized the relative kinetics of parental histone mobilization and new histone deposition upon local UVC damage (Figure 4A) in U2OS cells stably expressing H3.3-SNAP, allowing us to label parental and new histones in different colors within the same sample (see Experimental procedures for details). Parental histones H3.3 are displaced within minutes after damage induction, as described earlier, whereas new histone H3.3 accumulation at damage sites becomes detectable only 45 minutes after local UVC irradiation. We obtained similar results when we swapped the SNAP reagents, labeling old H3.3 in green and new H3.3 in red (data not shown). Thus, parental histone displacement precedes new histone deposition at UVC damage sites.

Given that the H3.3 histone chaperone HIRA promotes the deposition of newly synthesized H3.3 at UVC damage sites (Adam et al., 2013), we next tested whether the same chaperone was also responsible for parental H3.3 mobilization in UVC-damaged regions. Interestingly, HIRA depletion did not impair old H3.3 signal loss at UVC sites (Figure 4B), showing that this histone chaperone does not participate in parental H3.3 redistribution after UVC irradiation. These findings indicate that parental H3.3 mobilization occurs independently of

new H3.3 deposition. Consistent with this, preventing synthesis of new histones H3.3 by siRNA did not interfere with parental H3.3 displacement from UVC damaged regions (Figure 4C; note that this treatment did not affect pre-existing histone H3.3 levels because histones are very stable proteins). This experiment thus confirms that newly synthesized histone H3.3 dynamics have no impact on parental H3.3 mobilization in the vicinity of DNA damage. Altogether, these data demonstrate that parental histone H3.3 dynamics are functionally independent of new H3.3 deposition at UVC damage sites.

Recovery of parental histones coupled to repair progression through DDB2 release

Because parental histones are kept in the vicinity of UVC-damaged regions early after DNA damage, we decided to investigate whether and to which extent they contribute to chromatin restoration long-term after damage. For this purpose, we examined both parental and new H3.3 dynamics in parallel with repair progression at late time points after UVC laser micro-irradiation in U2OS cells stably expressing H3.3-SNAP and CFP-XPC (see Figure S4A for a characterization of the cell line). This revealed a 80% recovery of parental H3.3 histones at UVC damaged sites within 9 to 12 hours after irradiation (Figure 5A). In contrast, only 20% of parental H3.3 histones were mobile in undamaged chromatin within the same time frame (Figure S4B), consistent with a previous report (Kimura and Cook, 2001), arguing that parental H3.3 recovery in damaged chromatin does not result from basal histone turnover but actually reflects enhanced dynamics of parental histones in UVC-damaged regions. Similar results were obtained when we performed the experiment in the presence of an excess of non-fluorescent SNAP reagent to make sure that only parental histones were labeled in red (data not shown). Parental histone recovery at UVC damage sites was also recapitulated in U2OS cells stably expressing H3.3-PA-GFP (Figure S4C). Importantly, new histones deposited in damaged chromatin persisted while parental histones recovered (Figure 5A). Thus, our data establish that, long term after UVC irradiation, most parental histones recover and mix with newly synthesized histones in damaged chromatin.

We next sought to determine if parental H3.3 recovery in damaged chromatin was coupled to repair progression. For this, we depleted the late repair factor XPG, which interferes with repair progression with no major effect on the early mobilization of parental histones from damaged chromatin as shown above (Figure S3). Parental H3.3 recovery however was markedly impaired in XPG-depleted cells, reaching only 20% 9 hours after local UVC irradiation (Figure 5B). These results indicate that parental histone recovery in damaged chromatin is dependent on repair progression. Given that XPG depletion also significantly delayed DDB2 release from chromatin, we decided to assess more directly the role of DDB2 in parental histone recovery. For this, we triggered LacR-DDB2 release from the LacO array by adding IPTG to the culture medium (Figure 5C). We found that DDB2 release from

chromatin resulted in rapid recovery of old H3.3 density at the LacO array, which highlights the key role of DDB2 in controlling parental histone dynamics in UVC-damaged chromatin. Collectively, our results demonstrate the major contribution of parental histones to chromatin restoration coupled to repair and establish that parental histone recovery is coordinated with repair progression through DDB2 release from damaged chromatin.

DISCUSSION

By exploiting real-time tracking of parental H3 histones after local UVC damage in human cells, we provide novel insights into epigenome maintenance in response to DNA damage. Our study indeed identifies a conservative pathway, tightly coordinated with repair progression, whereby pre-existing histones are rapidly redistributed to the vicinity of UVC-damaged chromatin and subsequently recover (Figure 5D). We propose that the original information conveyed by parental histones is thus kept in the vicinity of the damaged areas in order to be restored after DNA repair, contributing to build a memory of chromatin identity in response to DNA damage.

Parental histone mobilization away from damaged chromatin regions

Chromatin disorganization coupled to the early stages of the DDR, although considered to be critical for efficient DNA repair, has remained essentially an uncharacterized process. Here, we provide evidence for a conservative redistribution of parental histones near damaged chromatin regions. Our findings thus argue against the commonly held view that histones are evicted from damaged chromatin to facilitate repair, prompting us to propose a revised version of the “Access-Repair-Restore” model. Even though histone solubilization has been reported in response to genotoxic stress (Goldstein et al., 2013; Wang et al., 2006; Xu et al., 2010), our data support a model where pre-existing histones are mobilized away from damaged chromatin regions mostly by nucleosome sliding and/or chromatin opening. Furthermore, whether this directly facilitates access to damaged DNA and repair progression is not entirely clear. Indeed, in conditions where ubiquitylation at damage sites is abrogated, the recruitment of the early NER factor XPC is impaired (Marteijn et al., 2014; Nouspikel, 2011) but parental histone mobilization is not. These findings argue that mobilizing parental histones is not sufficient for promoting the recruitment of NER factors to damaged chromatin. Keeping parental histones near the damaged region may favor the reorganization of chromatin after repair. It might also contribute to protect parental histones from modifications by enzymes recruited to regions of ongoing repair, thus promoting the maintenance of the original information. It will be of major interest to test this model further by investigating the functional relevance of parental histone mobilization in damaged chromatin.

The extent of chromatin rearrangements in response to local DNA damage infliction is another matter of debate. Although one study indicates that chromatin destabilization affects the whole nucleus upon local UVC irradiation (Rubbi and Milner, 2003), several lines of evidence rather support the idea that chromatin is locally disorganized upon genotoxic stress (Dinant et al., 2013; Goldstein et al., 2013; Hinde et al., 2014; Kruhlak et al., 2006; Luijsterburg et al., 2012; Smeenk et al., 2013). In line with this, here, we demonstrate that parental histones are redistributed to the vicinity of the UVC damaged area. It will be important to investigate the existence of structural barriers that would restrict the spreading of chromatin destabilization in response to DNA damage similar to boundary elements between chromatin domains. Furthermore, the extent of chromatin disorganization after DNA damage may be different in highly transcribed euchromatin regions compared to mostly silent heterochromatin, and is also likely to differ depending on the type of DNA lesion and repair pathway at work. It will thus be interesting to explore in future studies how the original chromatin state and the nature of the damage impact repair-coupled histone dynamics.

Regarding the mechanisms underlying chromatin disorganization in response to DNA damage, we have identified the damage sensor DDB2 as a master regulator of parental histone mobilization at sites of UVC lesions. Interestingly, while the ubiquitylation activity of DDB2-containing complex is required for new histone deposition in UVC-damaged chromatin (Adam et al., 2013), it is dispensable for parental histone dynamics coupled to UVC lesion recognition. Consistent with our findings, ubiquitylation-deficient mutants of DDB2 induce chromatin expansion like wild-type DDB2 when artificially tethered to chromatin in absence of DNA damage (Luijsterburg et al., 2012). Thus, DDB2-mediated parental histone mobilization and chromatin expansion at UVC damage sites is largely independent of the other members of the UVC damage recognition complex. Whether DDB2 acts alone or in association with other factors to fulfill this activity will be interesting to investigate in future studies. Remarkably, DDB2 has very strong affinity for UVC-damaged DNA (Kulaksiz et al., 2005; Wittschieben et al., 2005) which might be sufficient for moving nucleosomes away from damaged areas. However, structural studies have revealed that DDB2 binding to damaged DNA is still compatible with DNA wrapping around histone proteins within nucleosomes (Scrima et al., 2008; Yeh et al., 2012), suggesting that DDB2 binding might not be enough to promote nucleosome sliding. Given that the DDB2 protein does not display any ATPase/helicase nor histone binding domains, we rather favor a model where DDB2 works in concert with other factors directly involved in chromatin dynamics – such as histone chaperones and/or chromatin remodeling complexes that remain to be identified – to promote chromatin disorganization in damaged regions.

Epigenome maintenance after DNA damage

Our study identifies a critical pathway that contributes to preserving the integrity of chromatin

architecture in response to DNA damage. We unraveled that damaged chromatin reorganization is a two-step process with new histone incorporation preceding parental histone recovery in damaged chromatin regions. The biphasic nature of chromatin restoration is consistent with an early model based on the accessibility to nucleases of chromatin undergoing NER (reviewed in (Smerdon, 1991)).

Our findings have also broad implications for understanding how a memory of the initial epigenome is preserved in response to genotoxic stress. Indeed, we provide evidence that most parental histones recover and mix with newly synthesized histones in repairing chromatin. If newly synthesized histones persist in the repaired chromatin, how parental marks are transferred to the new histones that initially carry their own set of post-translational modifications (PTMs) (Loyola et al., 2006) is an open question. In this respect, a parallel can be drawn between the restoration of damaged chromatin and the reorganization of replicated chromatin, in which parental histones are recycled and new histones are deposited (Alabert and Groth, 2012; MacAlpine and Almouzni, 2013). However, while cells have to cope with 50% histone renewal during replication, most parental histones recover in damaged chromatin regions, which could facilitate the re-establishment of the original chromatin landscape. Following DNA replication, the maintenance of chromatin identity is achieved by old histone recycling with their PTMs at the replication fork and by subsequent modifications of new histones to mirror the parental ones (Alabert et al., 2015). Whether similar mechanisms operate in damaged chromatin and whether parental and new histones are mixed together in a same nucleosome to facilitate old PTM transmission to newly deposited histones will be addressed in future studies.

Finally, our data open up new avenues for understanding the etiology of several human diseases including H3 mutant-associated cancers (reviewed in (Kallappagoudar et al., 2015; Yuen and Knoepfler, 2013)) and NER disorders (reviewed in (DiGiovanna and Kraemer, 2012; Marteijn et al., 2014)). Given that DDB2 dynamics strongly impact the fate of parental histones in response to UVC damage, it will be important to consider that the phenotype of XPE patients harboring DDB2 mutations may not only reflect a DNA repair deficiency but could also be a consequence of altered chromatin plasticity in response to genotoxic stress. Similarly, H3 mutations could contribute to the development of human cancers by affecting the resetting of the epigenome in response to DNA damage.

In conclusion, our work sheds new light to our current view of DNA damage-induced chromatin rearrangements, with parental histone dynamics playing a major role in the maintenance of epigenome integrity in response to genotoxic stress. Our findings also pave the way for the identification of new factors that contribute to restoring damaged chromatin identity, thus protecting cells against pathological conditions.

EXPERIMENTAL PROCEDURES

Cell culture and drug treatments

All U2OS cell lines were grown at 37°C and 5% CO₂ in Dulbecco's modified Eagle's medium (DMEM, Invitrogen) supplemented with 10% fetal calf serum (EUROBIO), 100 U/mL penicillin and 100 µg/mL streptomycin (Invitrogen) and the appropriate selection antibiotics (Table S1).

DNA was stained by incubating live cells with Hoechst 33258 (10 µg/mL final concentration, Sigma-Aldrich) for 30 min at 37°C before the analysis. Detergent extraction on live cells was performed as described in the immunofluorescence section of the Supplemental experimental procedures. Proteasome inhibition was performed by adding MG132 to the culture medium for 2 h at 37°C before the analysis (10 µM final concentration, Enzo Life Science). LacR-DDB2 release from the Lac operator was achieved by adding IPTG (isopropyl β-D-1-thiogalactopyranoside, 10 µM final concentration, Euromedex) to the culture medium in which the usual serum is replaced by Tetracycline-free fetal calf serum (Biowest). For long-term experiments on live cells, Hepes buffer was added to the culture medium (25 mM final concentration, Sigma-Aldrich).

SNAP labeling and photo-activation of histones

Pre-existing SNAP-tagged histones were labeled by incubating cells with 2 µM SNAP-cell TMR star (New England Biolabs) for 20 min (pulse), followed by a 30 min-incubation in fresh medium. Cells were subject to laser micro-irradiation 48 h after the pulse.

For specific labeling of newly-synthesized histones, pre-existing SNAP-tagged histones were first quenched by incubating cells with 10 µM SNAP-cell Block (New England Biolabs) for 30 min followed by a 30 min-wash in fresh medium and a 2 h-chase. The SNAP-tagged histones neo-synthesized during the chase were then pulse-labeled with 4 µM SNAP-cell Oregon Green (New England Biolabs) for 20 min followed by a 30 min-incubation in fresh medium. Cells were subject to local UVC irradiation immediately afterwards.

Photo-activation experiments were performed in U2OS cells stably expressing H3.3-PA-GFP on a Zeiss LSM710 confocal microscope using the 405 nm laser focused through a LD LCI Plan-Apochromat 25x/0.8 oil objective (laser settings: maximum power, 5 iterations, 6.30 µsec/pixel scan speed). We photo-activated either total nuclei 48 h prior to local UVC irradiation or a nuclear region of 20 µm² 8 to 10 h before local UVC irradiation to minimize the distortion of the photo-activated area due to cell movement and cell division.

FRAP

Bleaching of the red fluorescence was performed with a 555 nm laser (laser settings: maximum power, 4 iterations, 1.58 µsec/pixel scan speed). Bleaching of the green

fluorescence was performed using a 488 nm laser (laser settings: maximum power, 15 iterations, 6.30 μ sec/pixel scan speed). In both cases, the laser was focused through a LD LCI Plan-Apochromat 25x/0.8 multi-immersion objective, the bleached area was 2 μ m in diameter and bleaching conditions were set to reach a local loss of fluorescence similar to the loss of signal observed 15 min after UVC laser damage. For bleaching of the red fluorescence in the entire nucleus to leave a small fluorescent patch of 20 μ m², the laser settings were changed to 10 iterations and 12.61 μ sec/pixel scan speed.

siRNA and plasmid transfections

siRNAs purchased from Eurofins MWG Operon (Table S2) were transfected into cells using Lipofectamine RNAiMAX (Invitrogen) following manufacturer's instructions. The final concentration of each siRNA in the culture medium was 50 nM. Cells were analyzed and/or harvested 72 h post-transfection. When performing over-night experiments with mixed cell populations treated with different siRNAs, one of the two cell populations was stained with Cell Tracker Deep Red (Life Technologies) following manufacturer's instructions.

Cells were transiently transfected with plasmid DNA (1 μ g/ml final) using Lipofectamine 2000 (Invitrogen) according to manufacturer's instructions 48 h before subsequent cell treatment. For stable cell line establishment, cells were transfected with plasmid DNA as above 48 h before antibiotic selection of clones. All constructs were verified by direct sequencing and/or restriction digests. Cloning details and primer sequences (Sigma-Aldrich) are available upon request. Plasmids are described in Table S3.

UVC laser micro-irradiation

For laser-induction of UVC damage (Dinant et al., 2007), cells were grown on quartz coverslips (SPI supplies) and irradiated for 50 ms unless stated otherwise using a 2 mW pulsed diode-pumped solid-state laser emitting at 266 nm (repetition rate up to 10 kHz, Rapp OptoElectronics, Hamburg GmbH). The laser was attenuated using a neutral density filter OD1 and focused through a 40x/0.6 Ultrafluar glycerol objective. In these conditions, UVC laser damage did not cause major cytotoxicity as the mortality rate over a 14 h live cell imaging experiment after laser damage was only around 10% and damaged cells did repair and went through mitosis.

Cell extracts and western blot

Total extracts were obtained by scraping cells in Laemmli buffer (50 mM Tris HCl pH 6.8, 1.6% SDS (Sodium Dodecyl Sulfate), 8% glycerol, 4% β -mercaptoethanol, 0.0025% bromophenol blue) followed by 5 min denaturation at 95°C. For western blot analysis, extracts were run on 4%–20% Mini-PROTEAN TGX gels (Bio-Rad) in running buffer (200 mM glycine, 25 mM Tris, 0.1% SDS) and transferred onto nitrocellulose membranes

(Protran) with a Trans-Blot SD semidry transfer cell (Bio-Rad). Total proteins were revealed by reversible protein stain (Pierce). Proteins of interest were probed using the appropriate primary and HRP (Horse Radish Peroxidase)-conjugated secondary antibodies (Jackson Immunoresearch), detected using Super-Signal West Pico or Femto chemiluminescence substrates (Pierce) (see Table S4 for the list of antibodies).

Quantitative RT-PCR

RNA extracted from cells with Trizol (Invitrogen) and precipitated in isopropanol was subject to DNA digestion with Turbo DNA-free (Life technologies) and reverse transcribed with Superscript III RT using random primers (Life technologies). Quantitative PCR reactions were carried out with the indicated primer pairs (Table S5) and the Power SYBR® Green PCR Master Mix (Life Technologies) and read in 96-well plates (MicroAmp® Fast Optical, Life Technologies) using a ABI 7500 Fast detection system (Life Technologies). Results were normalized to the amount of the GAPDH gene product.

Image acquisition and analysis

Live cell imaging of LacR-DDB2 dynamics was performed on a Zeiss LSM710 confocal microscope using a Plan-APOCHROMAT 63x/1.4 oil objective. Live cell imaging coupled to local UVC irradiation was performed using a LD LCI Plan-APOCHROMAT 25x/0.8 multi-immersion objective on a Zeiss LSM 700 confocal microscope adapted for UVC transmission with all-quartz optics. The fluorescence-based autofocus mode was activated in order to acquire images from the best focal plane. Image J software was used for image analysis. To correct for overall bleaching of the signal due to repetitive imaging, fluorescence intensities were normalized against intensities measured in an undamaged nucleus in the same field. The extent of fluorescence loss at irradiated sites was determined by dividing the fluorescence intensity in the illuminated area by the fluorescence intensity of the entire nucleus, after background subtraction. The illuminated area was defined at 10-15 min post irradiation, based on fluorescently-labeled XPC or based on fluorescence loss, and was kept the same for all time points. Fluorescence recovery in the illuminated region was calculated relative to before illumination and starting from the time point with minimum intensity. 2D projections of 3D images from z-stack acquisitions were obtained by maximum intensity z-projection. On these projections, fluorescence intensity was measured in the micro-irradiated zone, in the entire nucleus and in concentric regions spaced by 1 pixel and centered on the laser micro-irradiation site using a custom macro.

Statistical analysis

p-values from at least two independent experiments were calculated with a student t-test, including Welch's correction when necessary, using R software.

AUTHOR CONTRIBUTIONS

S.A. and J.D. contributed equally to this work. S.A., J.D. and S.E.P designed and performed experiments, analyzed the data and wrote the manuscript. O.C. provided technical assistance. O.L. and O.R. helped with UVC laser micro-irradiation and computational analyses of imaging data. S.E.P and G.A. supervised the project.

ACKNOWLEDGMENTS

We thank N. Dantuma, E. Dunleavy, J. Lippincott-Schwartz and R. Nishi for sharing reagents. We acknowledge the Imagoseine imaging Facility (Paris Diderot University) for assistance with confocal microscopy. This work was supported by the European Research Council (ERC starting grant ERC-2013-StG-336427 "EpIn"), the French National Research Agency (ANR-12-JSV6-0002-01), the "Who am I?" laboratory of excellence (ANR-11-LABX-0071) funded by the French Government through its "Investments for the Future" program (ANR-11-IDEX-0005-01), EDF Radiobiology program RB 2014-01 and the Fondation ARC. Research in GA laboratory is supported by la Ligue Nationale contre le Cancer (Equipe labellisée Ligue), the European Commission Network of Excellence EpiGeneSys (HEALTH-F4-2010-257082), ERC Advanced Grant 2009-AdG_20090506 "Eccentric", the European Commission large-scale integrating project FP7_HEALTH-2010-259743 "MODHEP", ANR "ChromaTin" ANR-10-BLAN-1326-03, ANR-11-LABX-0044_DEEP and ANR-10-IDEX-0001-02 PSL*, ANR "CHAPINHIB" ANR-12-BSV5-0022-02 and Aviesan-ITMO cancer project "Epigenomics of breast cancer". S.A. is the recipient of a PhD fellowship from University Pierre et Marie Curie and La Ligue contre le Cancer. J.D. is the recipient of a PhD fellowship from University Paris Diderot.

REFERENCES

- Adam, S., Polo, S.E., and Almouzni, G. (2013). Transcription Recovery after DNA Damage Requires Chromatin Priming by the H3.3 Histone Chaperone HIRA. *Cell* *155*, 94–106.
- Alabert, C., and Groth, A. (2012). Chromatin replication and epigenome maintenance. *Nat. Rev. Mol. Cell Biol.* *13*, 153–167.
- Alabert, C., Barth, T.K., Reverón-Gómez, N., Sidoli, S., Schmidt, A., Jensen, O.N., Imhof, A., and Groth, A. (2015). Two distinct modes for propagation of histone PTMs across the cell cycle. *Genes Dev.* *29*, 585–590.
- Alekseev, S., and Coin, F. (2015). Orchestral maneuvers at the damaged sites in nucleotide excision repair. *Cell. Mol. Life Sci.* doi : 10.1007/s00018-015-1859-5.

Bannister, A.J., and Kouzarides, T. (2011). Regulation of chromatin by histone modifications. *Cell Res.* *21*, 381–395.

Ciccia, A., and Elledge, S.J. (2010). The DNA damage response: making it safe to play with knives. *Molecular Cell* *40*, 179–204.

DiGiovanna, J.J., and Kraemer, K.H. (2012). Shining a light on xeroderma pigmentosum. *J. Invest. Dermatol.* *132*, 785–796.

Dinant, C., Ampatziadis-Michailidis, G., Lans, H., Tresini, M., Lagarou, A., Grosbart, M., Theil, A.F., van Cappellen, W.A., Kimura, H., Bartek, J., et al. (2013). Enhanced chromatin dynamics by FACT promotes transcriptional restart after UV-induced DNA damage. *Molecular Cell* *51*, 469–479.

Dinant, C., de Jager, M., Essers, J., van Cappellen, W.A., Kanaar, R., Houtsmuller, A.B., and Vermeulen, W. (2007). Activation of multiple DNA repair pathways by sub-nuclear damage induction methods. *Journal of Cell Science* *120*, 2731–2740.

Dunleavy, E.M., Almouzni, G., and Karpen, G.H. (2011). H3.3 is deposited at centromeres in S phase as a placeholder for newly assembled CENP-A in G₁ phase. *Nucleus* *2*, 146–157.

Goldstein, M., Derheimer, F.A., Tait-Mulder, J., and Kastan, M.B. (2013). Nucleolin mediates nucleosome disruption critical for DNA double-strand break repair. *Proc Natl Acad Sci U S A* *110*, 16874–16879.

Green, C.M., and Almouzni, G. (2002). When repair meets chromatin. First in series on chromatin dynamics. *EMBO Rep.* *3*, 28–33.

Hinde, E., Kong, X., Yokomori, K., and Gratton, E. (2014). Chromatin Dynamics during DNA Repair Revealed by Pair Correlation Analysis of Molecular Flow in the Nucleus. *Biophys. J.* *107*, 55–65.

Hoeijmakers, J.H.J. (2009). DNA damage, aging, and cancer. *N. Engl. J. Med.* *361*, 1475–1485.

Jackson, S.P., and Bartek, J. (2009). The DNA-damage response in human biology and disease. *Nature* *461*, 1071–1078.

Kallappagoudar, S., Yadav, R.K., Lowe, B.R., and Partridge, J.F. (2015). Histone H3 mutations-a special role for H3.3 in tumorigenesis? *Chromosoma*. doi: 10.1007/s00412-015-0510-4.

- Kimura, H., and Cook, P.R. (2001). Kinetics of core histones in living human cells: little exchange of H3 and H4 and some rapid exchange of H2B. *J. Cell Biol.* *153*, 1341–1353.
- Kornberg, R.D. (1977). Structure of chromatin. *Annu. Rev. Biochem.* *46*, 931–954.
- Kruhlak, M.J., Celeste, A., Dellaire, G., Fernandez-Capetillo, O., Müller, W.G., McNally, J.G., Bazett-Jones, D.P., and Nussenzweig, A. (2006). Changes in chromatin structure and mobility in living cells at sites of DNA double-strand breaks. *J. Cell Biol.* *172*, 823–834.
- Kulaksiz, G., Reardon, J.T., and Sancar, A. (2005). Xeroderma pigmentosum complementation group E protein (XPE/DDB2): purification of various complexes of XPE and analyses of their damaged DNA binding and putative DNA repair properties. *Molecular and Cellular Biology* *25*, 9784–9792.
- Lan, L., Nakajima, S., Kapetanaki, M.G., Hsieh, C.L., Fagerburg, M., Thickman, K., Rodriguez-Collazo, P., Leuba, S.H., Levine, A.S., and Rapić-Otrin, V. (2012). Monoubiquitinated histone H2A destabilizes photolesion-containing nucleosomes with concomitant release of UV-damaged DNA-binding protein E3 ligase. *J. Biol. Chem.* *287*, 12036–12049.
- Loyola, A., Bonaldi, T., Roche, D., Imhof, A., and Almouzni, G. (2006). PTMs on H3 variants before chromatin assembly potentiate their final epigenetic state. *Molecular Cell* *24*, 309–316.
- Luijsterburg, M.S., Lindh, M., Acs, K., Vrouwe, M.G., Pines, A., van Attikum, H., Mullenders, L.H., and Dantuma, N.P. (2012). DDB2 promotes chromatin decondensation at UV-induced DNA damage. *J. Cell Biol.* *197*, 267–281.
- MacAlpine, D.M., and Almouzni, G. (2013). Chromatin and DNA replication. *Cold Spring Harb Perspect Biol* *5*, a010207.
- Marteijn, J.A., Lans, H., Vermeulen, W., and Hoeijmakers, J.H.J. (2014). Understanding nucleotide excision repair and its roles in cancer and ageing. *Nat. Rev. Mol. Cell Biol.* *15*, 465–481.
- Maze, I., Noh, K.-M., Soshnev, A.A., and Allis, C.D. (2014). Every amino acid matters: essential contributions of histone variants to mammalian development and disease. *Nat. Rev. Genet.* *15*, 259–271.
- Nouspikel, T. (2011). Multiple roles of ubiquitination in the control of nucleotide excision repair. *Mech. Ageing Dev.* *132*, 355–365.

Polo, S.E., Roche, D., and Almouzni, G. (2006). New histone incorporation marks sites of UV repair in human cells. *Cell* *127*, 481–493.

Probst, A.V., Dunleavy, E., and Almouzni, G. (2009). Epigenetic inheritance during the cell cycle. *Nat. Rev. Mol. Cell Biol.* *10*, 192–206.

Rubbi, C.P., and Milner, J. (2003). p53 is a chromatin accessibility factor for nucleotide excision repair of DNA damage. *Embo J.* *22*, 975–986.

Scrima, A., Konícková, R., Czyzewski, B.K., Kawasaki, Y., Jeffrey, P.D., Groisman, R., Nakatani, Y., Iwai, S., Pavletich, N.P., and Thomä, N.H. (2008). Structural basis of UV DNA-damage recognition by the DDB1-DDB2 complex. *Cell* *135*, 1213–1223.

Smeenk, G., Wiegant, W.W., Marteijn, J.A., Luijsterburg, M.S., Sroczynski, N., Costelloe, T., Romeijn, R.J., Pastink, A., Mailand, N., Vermeulen, W., et al. (2013). Poly(ADP-ribosyl)ation links the chromatin remodeler SMARCA5/SNF2H to RNF168-dependent DNA damage signaling. *Journal of Cell Science* *126*, 889–903.

Smerdon, M.J. (1991). DNA repair and the role of chromatin structure. *Curr. Opin. Cell Biol.* *3*, 422–428.

Soria, G., Polo, S.E., and Almouzni, G. (2012). Prime, repair, restore: the active role of chromatin in the DNA damage response. *Molecular Cell* *46*, 722–734.

Talbert, P.B., and Henikoff, S. (2010). Histone variants--ancient wrap artists of the epigenome. *Nat. Rev. Mol. Cell Biol.* *11*, 264–275.

Wang, H., Zhai, L., Xu, J., Joo, H.-Y., Jackson, S., Erdjument-Bromage, H., Tempst, P., Xiong, Y., and Zhang, Y. (2006). Histone H3 and H4 ubiquitylation by the CUL4-DDB-ROC1 ubiquitin ligase facilitates cellular response to DNA damage. *Molecular Cell* *22*, 383–394.

Wittschieben, B.Ø., Iwai, S., and Wood, R.D. (2005). DDB1-DDB2 (xeroderma pigmentosum group E) protein complex recognizes a cyclobutane pyrimidine dimer, mismatches, apurinic/apyrimidinic sites, and compound lesions in DNA. *J. Biol. Chem.* *280*, 39982–39989.

Xu, Y., Sun, Y., Jiang, X., Ayrapetov, M.K., Moskwa, P., Yang, S., Weinstock, D.M., and Price, B.D. (2010). The p400 ATPase regulates nucleosome stability and chromatin ubiquitination during DNA repair. *J. Cell Biol.* *191*, 31–43.

Yeh, J.I., Levine, A.S., Du, S., Chinte, U., Ghodke, H., Wang, H., Shi, H., Hsieh, C.L.,

Conway, J.F., Van Houten, B., et al. (2012). Damaged DNA induced UV-damaged DNA-binding protein (UV-DDB) dimerization and its roles in chromatinized DNA repair. Proc Natl Acad Sci U S A 109, E2737–E2746.

Yuen, B.T.K., and Knoepfler, P.S. (2013). Histone H3.3 mutations: a variant path to cancer. Cancer Cell 24, 567–574.

FIGURE LEGENDS

Figure 1: Rapid mobilization of parental H3 histones from UVC-damaged chromatin regions.

(A) Current model for histone dynamics in UVC-damaged chromatin (left): the incorporation of new histones (green) raises questions about the fate of parental histones (red). The experimental strategy for tracking parental histone dynamics at DNA damage sites (right) combines SNAP-tag labeling of parental histones with local UVC damage by laser micro-irradiation and live cell imaging.

(B) Distribution of parental histones H3.3 (red) at the indicated time points after UVC laser micro-irradiation in U2OS cells stably expressing H3.3-SNAP and GFP-XPC (repair factor).

(C) Dynamics of parental histones H3.3 (red) at early time points after local damage with the UVC laser or local bleaching of the red fluorescence with a 555 nm laser in U2OS cells stably expressing H3.3-SNAP. UVC laser micro-irradiation was also applied to paraformaldehyde-fixed cells to control for photo-bleaching of the red fluorescence by the UVC laser. White arrowheads indicate the illuminated areas. Scale bars, 10 μ m. The graphs show quantifications of the red fluorescence associated with parental H3.3 in illuminated areas, normalized to the red fluorescence in the same areas before laser micro-irradiation. Error bars represent SD from n cells scored in two independent experiments.

See also Figure S1.

Figure 2: Conservative redistribution of parental histones to the vicinity of UVC-damaged regions.

(A) Experimental procedure for measuring parental histone loss and redistribution around the UVC damaged zone. A region of interest is defined by photo-bleaching of the red fluorescence associated with parental H3.3-SNAP histones leaving a small fluorescent patch in the nucleus, which is subjected to micro-irradiation with a 266 nm UVC laser (damage induction) or with a 555 nm bleaching laser (control). Fluorescence measurements are performed in the indicated regions on 2D projections of 3D acquisitions.

(B) Fluorescent patches of parental histones H3.3 (red) before and 15 min after local UVC damage (left) or local photo-bleaching (right) in U2OS cells stably expressing H3.3-SNAP

and GFP-XPC. Red dotted lines delineate the cell nuclei. The edges of the fluorescent patches of parental histones before and 15 min after local irradiation are shown in white on the zoomed images. The boxplots show quantification of the red fluorescence associated with parental H3.3-SNAP histones in the entire nucleus (left) or in the illuminated region (right) at 15 min normalized to before illumination (dotted line). n: number of cells

(C) Quantification of the red fluorescence associated with parental H3.3-SNAP histones in concentric regions around the UVC damage site (purple) or the site of fluorescence bleaching with the 555 nm laser (red) at the indicated time points.

(D) Difference in red fluorescence distribution between the two time points obtained by subtracting 0 min from 15 min values quantified in (C). The position of the repair zone is based on GFP-XPC accumulation at 15 min. Error bars represent SD from n cells scored in two independent experiments.

(E) Distribution of parental histones H3.3 (red) and DNA (blue, stained with Hoechst) 15 min after local UVC irradiation in U2OS cells stably expressing H3.3-SNAP. Paraformaldehyde-fixed cells were used as a control for photo-bleaching of Hoechst staining by the UVC laser. White arrowheads indicate the irradiated areas. The graphs show quantifications of fluorescence loss in irradiated areas (red fluorescence associated with parental H3.3 and blue fluorescence associated with DNA; data from n cells scored in two independent experiments).

Scale bars, 10 μ m.

See also Figure S2.

Figure 3: Parental histone redistribution is controlled by the repair factor DDB2

(A) Distribution of parental histones H3.3 15 min after UVC laser micro-irradiation at increasing UVC doses (exposure times to UVC are indicated) in U2OS cells stably expressing H3.3-SNAP and GFP-XPC.

(B) Scheme of the main repair factors involved in UVC damage detection in the global genome NER pathway.

(C) Distribution of parental histones H3.3 (red) 15 min after UVC laser micro-irradiation in U2OS cells stably expressing H3.3-SNAP and GFP-XPC treated with the indicated siRNAs (siLUC: control). siRNA efficiencies were verified by western-blot (right). The boxplots show quantifications of red fluorescence loss in irradiated areas at 15 min compared to before laser micro-irradiation (data from n cells scored in two independent experiments).

(D) Distribution of parental histones H3.3 (red) 15 min after UVC laser micro-irradiation in U2OS cells stably expressing H3.3-SNAP and GFP-XPC or GFP-DDB2. Expression levels of exogenous XPC and DDB2 relative to the endogenous proteins are shown on the western-blot panel (right). The boxplots show quantifications of red fluorescence loss in irradiated areas at 15 min compared to before laser micro-irradiation and of the area of fluorescence loss marked by GFP-tagged NER factors.

(E) Distribution of parental histones H3.3 (green) upon tethering of mCherry-LacR (-) or mCherry-LacR-DDB2 (DDB2) to the LacO array in U2OS LacO cells stably expressing H3.3-SNAP as depicted on the scheme (left). Quantifications of the area of the LacO array and the green fluorescence at the LacO array are displayed on the boxplots, which represent data from n cells scored in two independent experiments. White arrowheads indicate the irradiated areas or the position of the LacO array. Scale bars, 10 μ m.

See also Figure S3.

Figure 4: Parental H3.3 redistribution is independent of new H3.3 deposition.

(A) Dynamics of parental (red) and newly synthesized (green) histones H3.3 at the indicated time points after UVC laser micro-irradiation in U2OS cells stably expressing H3.3-SNAP. The graph shows quantifications of red and green fluorescence in irradiated areas, normalized to before laser micro-irradiation. Error bars represent SD from n cells scored in two independent experiments.

(B) Distribution of parental histones H3.3 (red) 15 min after UVC laser micro-irradiation in U2OS cells stably expressing H3.3-SNAP and GFP-XPC treated with the indicated siRNAs (siLUC: control). siRNA efficiency was verified by western-blot (bottom).

(C) Distribution of parental (red) and newly synthesized (green) histones H3.3 at the indicated time points after UVC laser micro-irradiation in U2OS cells stably expressing H3.3-SNAP treated with the indicated siRNAs (siLUC: control). siRNA efficiency was verified by quantitative RT-PCR (right). The boxplots show quantification of red fluorescence loss in irradiated areas at 15 min compared to before laser micro-irradiation (data from n cells scored in two independent experiments). White arrowheads indicate the irradiated areas. Scale bars, 10 μ m.

Figure 5: Recovery of parental histones coupled to repair progression

(A) Dynamics of parental (red) and newly synthesized histones H3.3 (green) at the indicated time points after UVC laser micro-irradiation in U2OS cells stably expressing H3.3-SNAP and CFP-XPC (blue). The graph shows quantification of red fluorescence recovery in irradiated areas. Cells that did not repair efficiently (based on CFP-XPC retention) were excluded from the analysis. Error bars represent SD from n cells scored in two independent experiments.

(B) Dynamics of parental histones H3.3 (red) at the indicated time points after UVC laser micro-irradiation in U2OS cells stably expressing H3.3-SNAP and GFP-DDB2 treated with the indicated siRNAs (siLUC: control). The efficiency of XPG depletion is indicated by sustained retention of GFP-DDB2 at UV sites. The graphs show quantification of red fluorescence recovery in irradiated areas. Error bars represent SD from n cells scored in two independent experiments.

(C) Distribution of parental H3.3 (green) upon IPTG-mediated release of mCherry-LacR-DDB2 from the LacO array in U2OS LacO cells stably expressing H3.3-SNAP. The graphs show quantifications of the green fluorescence at the LacO array and of the LacR-DDB2 area (red) after IPTG addition. Error bars represent SD from n cells scored in two independent experiments. White arrowheads indicate the irradiated areas or the position of the LacO array. Scale bars, 10 μ m.

(D) Model for parental histone dynamics in UVC-damaged chromatin regions.

See also Figure S4.

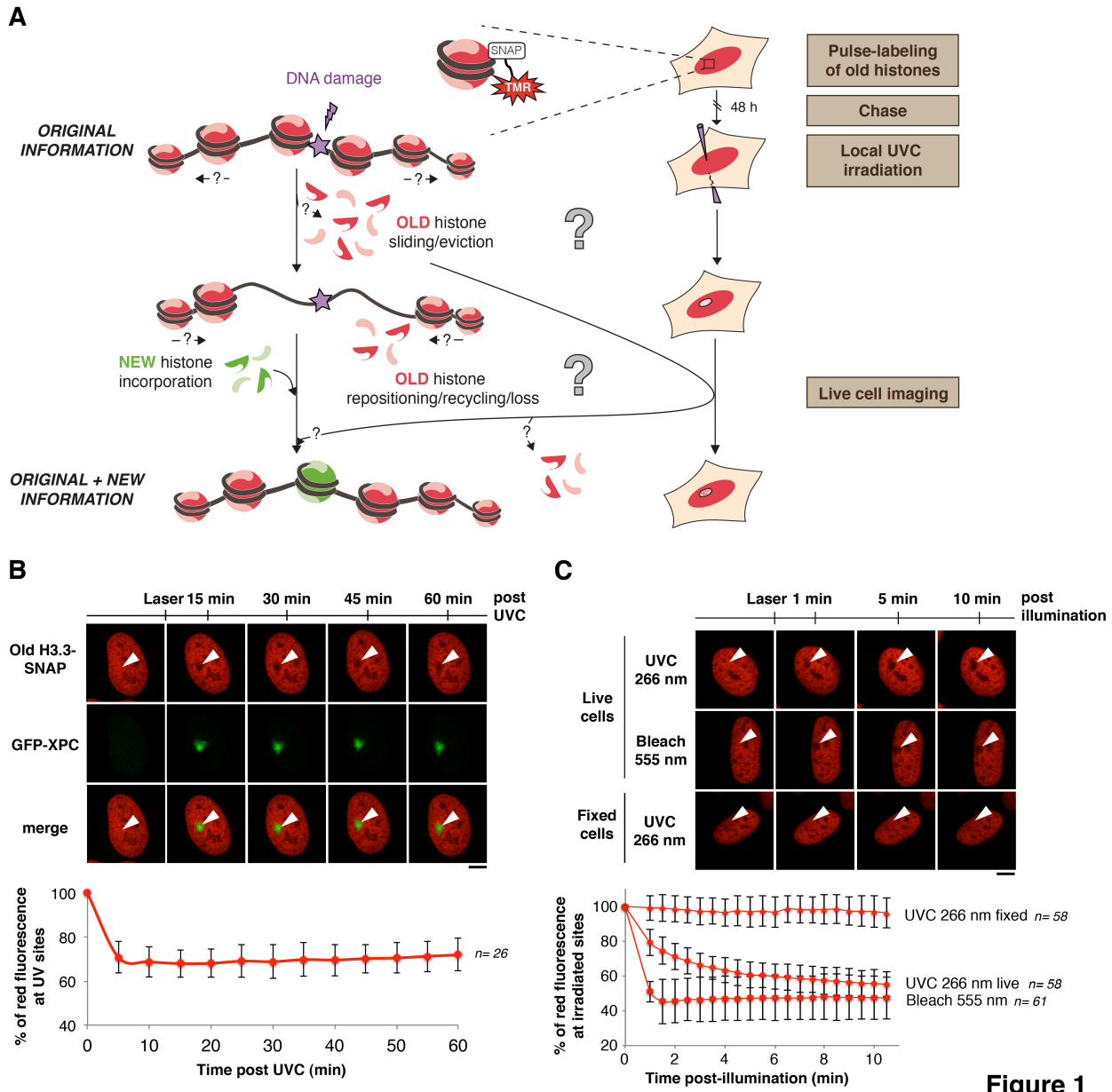


Figure 1

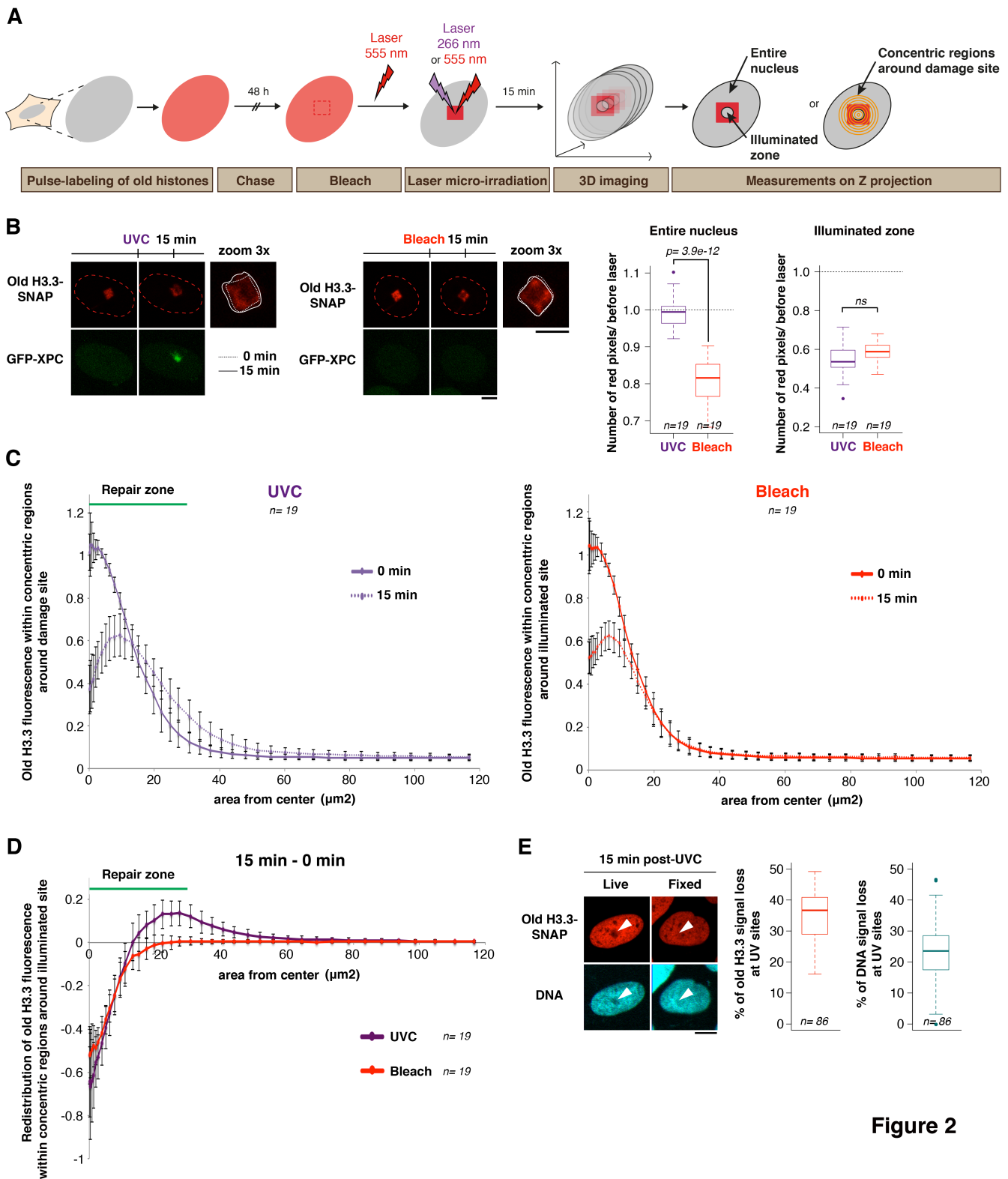


Figure 2

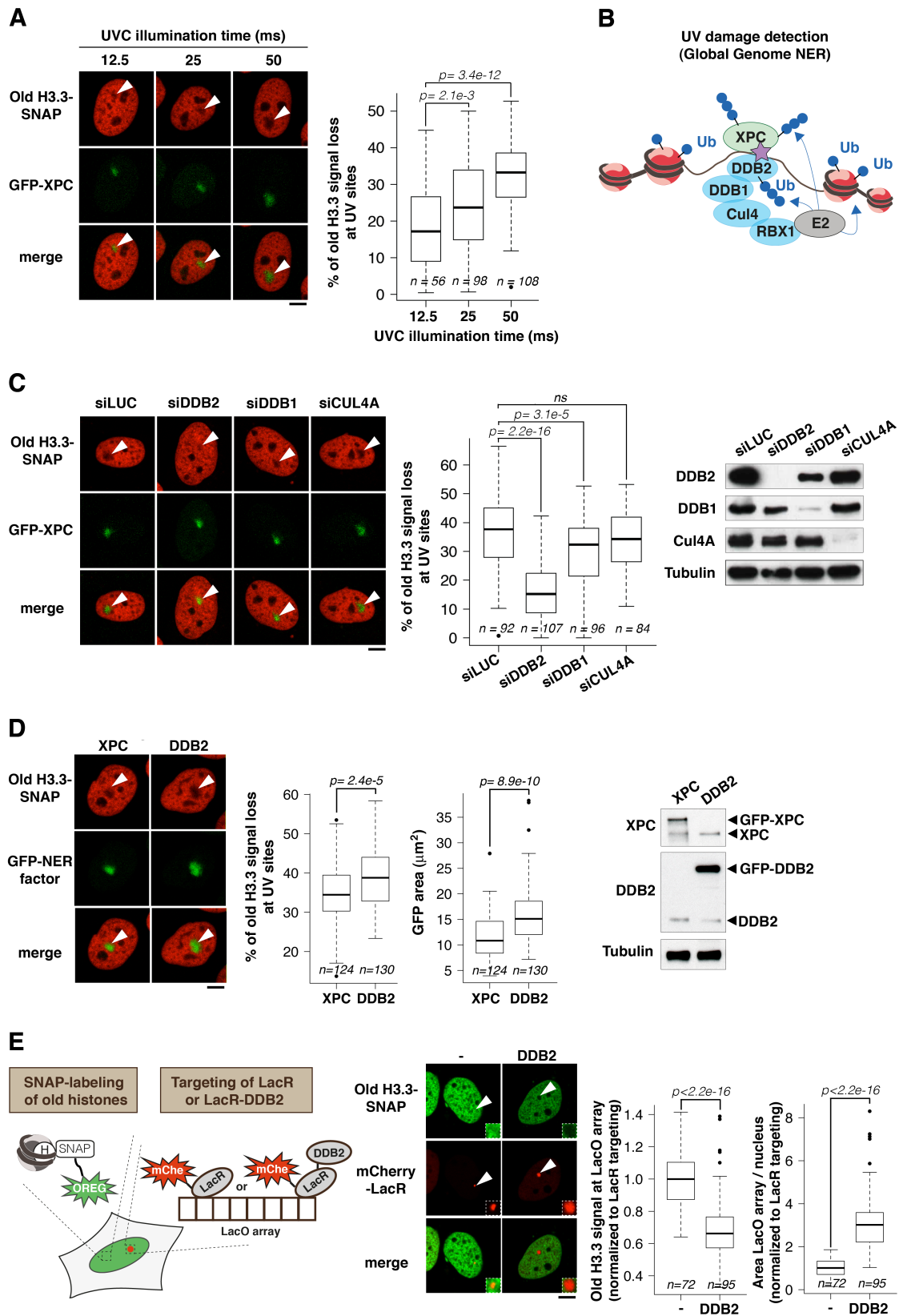


Figure 3

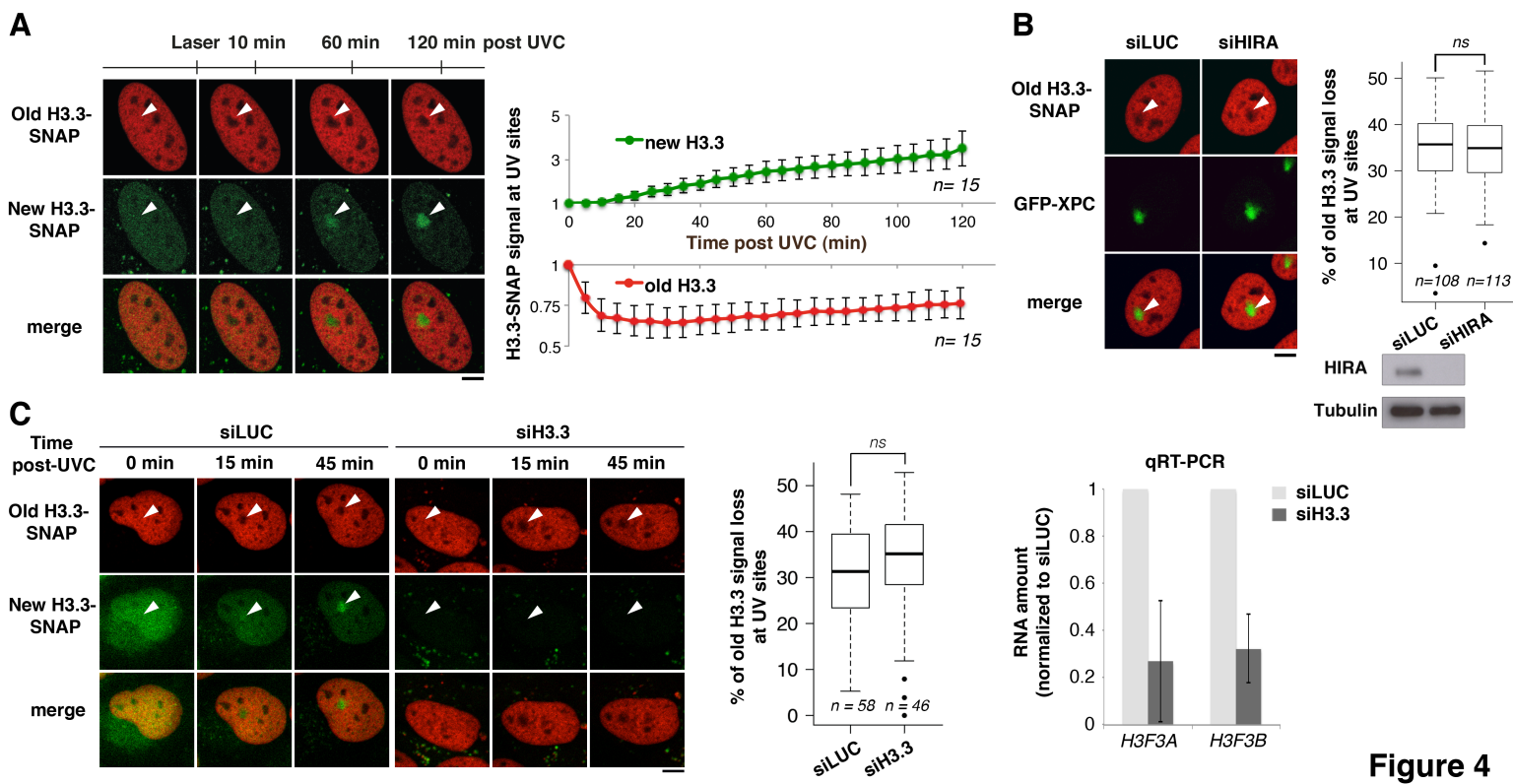


Figure 4

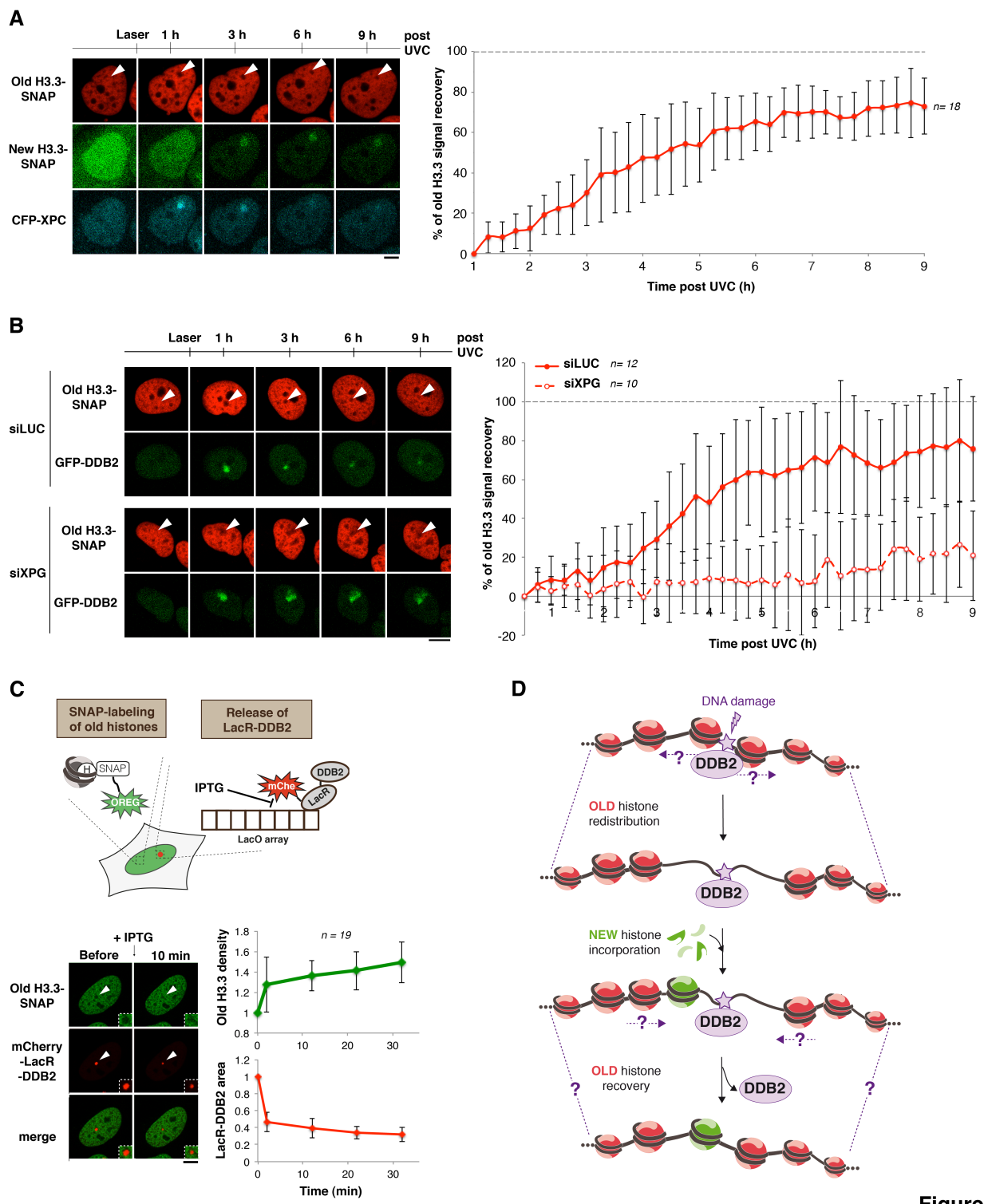


Figure 5

Supplemental Information

EXTENDED EXPERIMENTAL PROCEDURES

Local UVC irradiation (Katsumi et al., 2001; Moné et al., 2001)

Cells grown on glass coverslips (VWR) were covered with a polycarbonate filter (5 µm pore size, Millipore) and irradiated with 150 J/m² UVC (254 nm) using a low-pressure mercury lamp (Vilbert-Lourmat). Conditions were set using a VLX-3W dosimeter (Vilbert-Lourmat).

Immunofluorescence

Cells grown on glass coverslips (VWR) were either fixed directly with 2% paraformaldehyde and permeabilized with 0.2% Triton X-100 in PBS, or pre-extracted before fixation with 0.5% Triton X-100 in CSK buffer (Cytoskeletal buffer: 10 mM PIPES pH 7.0, 100 mM NaCl, 300 mM sucrose, 3 mM MgCl₂). Samples were blocked in 5% BSA (Bovine Serum Albumin, Sigma-Aldrich) in PBS supplemented with 0.1% Tween before incubation with primary antibodies and secondary antibodies conjugated to Alexa-Fluor 594 or 680 (Invitrogen) (see Table S4 for a description of the antibodies). Coverslips were mounted in Vectashield medium with DAPI (Vector laboratories) and cells were imaged with a Leica DMI6000 epifluorescence microscope using a 63x oil objective.

Cell line (reference)	Selection antibiotics
U2OS H3.3-SNAP (Dunleavy et al., 2011)	G418
U2OS H3.3-SNAP GFP	G418
U2OS H3.3-SNAP GFP-XPC	G418 + Hygromycin
U2OS H3.3-SNAP CFP-XPC	G418 + Hygromycin
U2OS H3.3-SNAP GFP-DDB2	G418 + Hygromycin
U2OS H3.1-SNAP GFP-XPC (U2OS H3.1 SNAP from (Dunleavy et al., 2011))	G418 + Hygromycin
U2OS H3.3-PA-GFP RFP-XPC	G418 + Hygromycin
U2OS LacO H3.3-SNAP (U2OS LacO from (Beuzer et al., 2014; Soutoglou et al., 2007))	G418

Table S1: Stable cell lines.

Antibiotics: G418 (100 µg/mL, Invitrogen), Hygromycin (200 µg/mL, Euromedex).

Designation	Target sequence
siCUL4A	5' GAAUCCUACUGCUGAUCGA ^{3'}
siDDB1	5' GCAAGGACCUGCUGUUUAU ^{3'}
siDDB2	5' UCACUGGGCUGAAGUUUA ^{3'} ,
siDDB2#2	5' UCAGUUCGCUUAUGAAUU ^{3'}
siERCC6	5' GAAGAGUUGUCAGUGAUUA ^{3'}
siH3.3	1:1 combination of siH3.3A: 5' CUACAAAAGCCGCUCGCAA ^{3'} and siH3.3B: 5' GCUAAGAGAGUCACCAUCAU ^{3'}
siHIRA	5' GGAGAUGACAAACUGAUUA ^{3'}
siLUC (Luciferase)	5' CGUACGCGGAAUACUUCGA ^{3'}
siXPG	5' GAAAGAAGAUGCUALAACGU ^{3'}

Table S2: siRNA sequences.

Plasmid	Construct details
H3.3-SNAP	<i>H3F3B</i> coding sequence cloned into pSNAPm (New England Biolabs) (Dunleavy et al., 2011)
H3.1-SNAP	<i>HIST1H3C</i> coding sequence cloned into pSNAPm (New England Biolabs) (Dunleavy et al., 2011)
H3.3-PA-GFP	<i>H3F3B</i> coding sequence in frame with PA-GFP in PA-GFP-N1 (Patterson and Lippincott-Schwartz, 2004) subcloned into pSNAPm replacing the SNAP tag sequence
GFP	pEGFP-C1 (Clontech)
GFP-PCNA	(Leonhardt et al., 2000)
GFP-XPC	Flag-GFP-XPC in pIREShyg (Clontech) (Nishi et al., 2009)
RFP-XPC	RFP from mRFP-C1 (Campbell et al., 2002) subcloned into CFP-XPC plasmid, replacing CFP
CFP-XPC	CFP-XPC (Montpellier Genomic Collections) subcloned into pBabe Hygro (Cell Biolabs)
GFP-DDB2	<i>DDB2</i> coding sequence (Montpellier Genomic Collections) subcloned into GFP-XPC plasmid, replacing XPC
mCherry-lacR	mCherry-lacR-NLS (Soutoglou and Misteli, 2008)
mCherry-lacR-DDB2	DDB2 in mCherry-lacR (Luijsterburg et al., 2012)

Table S3: Plasmids.

All the coding sequences for histone variants and repair factors are of human origin except lacR-fused DDB2, which is murine.

Type	Antibody	Species	Dilution	Application	Supplier (reference)
Primary	CUL4A	Rabbit	1:2000	WB	Bethyl Laboratories (A300-739A)
	DDB1	Rabbit	1:2000	WB	Abcam (ab21080)
	DDB2	Mouse	1:200	WB	Abcam (ab51017)
	DsRed	Rabbit	1:1000	WB	Clontech (632496)
	ERCC6	Rabbit	1:500	WB	Santa Cruz Biotechnology (sc-25370)
	GFP	Mouse	1:1000	WB	Roche Applied Science (11814460001)
	H3.3	Mouse	1:200	WB	Abnova (H00003021-M01)
	HIRA	Mouse	1:200	WB	Active Motif (39557)
	Nucleolin	Rabbit	1:1000	IF	Santa Cruz Biotechnology (sc-13057)
	SNAP	Rabbit	1:1000	WB	Pierce Antibodies (CAB4255)
	Tubulin	Mouse	1:10 000	WB	Sigma-Aldrich (T9026)
	XPC	Mouse	1:500	WB	Genetex (GTX70294)
	XPG	Mouse	1:50	IF	Merck Millipore (05-923)
Secondary	Anti-Mouse HRP	Goat	1:10 000	WB	Jackson Immunoresearch (115-035-068)
	Anti-Rabbit HRP	Donkey	1:10 000	WB	Jackson Immunoresearch (711-035-152)
	Anti-Rabbit 680	Goat	1:10 000	IF	Invitrogen (A21109)
	Anti-Mouse 594	Goat	1:10 000	IF	Invitrogen (A11032)

Table S4: Antibodies.

Designation	Sequence	Final concentration	Supplier
H3F3A_F	5' GATGGCAACTAAATGGTGTTC 3'	500 nM	Eurofins
H3F3A_R	5' CAGGAACACAGCACAGAACAG 3'		MWG
H3F3B_F	5' CAACCCAGAAGGCGAAGATA 3'		Operon

H3F3B_R	5' TTTCTCCTTGCCTCTGCTC ^{3'}		
GAPDH_F	5' CAAGGCTGTGGGCAAGGT ^{3'}		
GAPDH_R	5' GGAAGGCCATGCCAGTGA ^{3'}		

Table S5: PCR primers.

F : forward ; R : reverse.

SUPPLEMENTAL REFERENCES

- Beuzer, P., Quivy, J.-P., and Almouzni, G. (2014). Establishment of a replication fork barrier following induction of DNA binding in mammalian cells. *Cell Cycle* *13*, 1607–1616.
- Campbell, R.E., Tour, O., Palmer, A.E., Steinbach, P.A., Baird, G.S., Zacharias, D.A., and Tsien, R.Y. (2002). A monomeric red fluorescent protein. *Proc Natl Acad Sci USA* *99*, 7877–7882.
- Dunleavy, E.M., Almouzni, G., and Karpen, G.H. (2011). H3.3 is deposited at centromeres in S phase as a placeholder for newly assembled CENP-A in G₁ phase. *Nucleus* *2*, 146–157.
- Katsumi, S., Kobayashi, N., Imoto, K., Nakagawa, A., Yamashina, Y., Muramatsu, T., Shirai, T., Miyagawa, S., Sugiura, S., Hanaoka, F., et al. (2001). In situ visualization of ultraviolet-light-induced DNA damage repair in locally irradiated human fibroblasts. *The Journal of Investigative Dermatology* *117*, 1156–1161.
- Leonhardt, H., Rahn, H.P., Weinzierl, P., Sporbert, A., Cremer, T., Zink, D., and Cardoso, M.C. (2000). Dynamics of DNA replication factories in living cells. *J Cell Biol* *149*, 271–280.
- Luijsterburg, M.S., Lindh, M., Acs, K., Vrouwe, M.G., Pines, A., van Attikum, H., Mullenders, L.H., and Dantuma, N.P. (2012). DDB2 promotes chromatin decondensation at UV-induced DNA damage. *J Cell Biol* *197*, 267–281.
- Moné, M.J., Volker, M., Nikaido, O., Mullenders, L.H., van Zeeland, A.A., Verschure, P.J., Manders, E.M., and van Driel, R. (2001). Local UV-induced DNA damage in cell nuclei results in local transcription inhibition. *EMBO Rep* *2*, 1013–1017.
- Nishi, R., Alekseev, S., Dinant, C., Hoogstraten, D., Houtsmuller, A.B., Hoeijmakers, J.H.J., Vermeulen, W., Hanaoka, F., and Sugasawa, K. (2009). UV-DDB-dependent regulation of nucleotide excision repair kinetics in living cells. *DNA Repair (Amst)* *8*, 767–776.
- Patterson, G.H., and Lippincott-Schwartz, J. (2004). Selective photolabeling of proteins using photoactivatable GFP. *Methods* *32*, 445–450.

Soutoglou, Dorn, Sengupta, Jasin, Nussenzweig, Ried, Danuser, and Misteli (2007). Positional stability of single double-strand breaks in mammalian cells. *Nat Cell Biol* 9, 675-682.

Soutoglou, E., and Misteli, T. (2008). Activation of the Cellular DNA Damage Response in the Absence of DNA Lesions. *Science* 320, 1507-1510.

SUPPLEMENTAL FIGURE LEGENDS

Figure S1: Parental histone H3 dynamics in UVC-damaged chromatin regions. Related to Figure 1.

- (A)** Characterization by western blot of U2OS cell lines stably expressing H3.3-SNAP and GFP-XPC or H3.3-PAGFP and RFP-XPC. e: epitope tag, *: aspecific band.
- (B)** Immunostaining for nucleolin in U2OS cells stably expressing H3.3-SNAP and GFP-XPC fixed 15 min after UVC laser micro-irradiation. Parental H3.3-SNAP histones were labeled in red as in Figure 1. Fluorescence profiles along the line crossing the UVC-damaged area (white arrowhead) and a nucleolus (empty arrowhead) are displayed on the graphs.
- (C)** Scheme of the experimental strategy for tracking parental histone dynamics at DNA damage sites based on photo-activation of PA-GFP-tagged H3.3 histones in the whole nucleus 48 h before UVC laser micro-irradiation and live cell imaging.
- (D)** Distribution of parental histones H3.3 (green) at the indicated time points after UVC laser micro-irradiation in U2OS cells stably expressing H3.3-PA-GFP and RFP-XPC (repair factor).
- (E)** Dynamics of parental histones H3.3 (green) at early time points after local damage induced by UVC laser micro-irradiation as in (D). Paraformaldehyde-fixed cells were used as a control for photo-bleaching of the green fluorescence by the UVC laser. White arrowheads indicate the illuminated areas. The graphs show quantifications of the green fluorescence associated with parental H3.3 in illuminated areas, normalized to the green fluorescence in the same areas before laser micro-irradiation. Error bars represent SD from n cells scored in two independent experiments.
- (F)** Distribution of parental histones H3.3 (red) 15 min after UVC laser micro-irradiation in U2OS cells stably expressing H3.3-SNAP and transiently transfected with GFP-PCNA. PCNA focal pattern is characteristic of S phase cells.
- (G)** Distribution of parental histones H3.1 before and 15 min after UVC laser micro-irradiation in U2OS cells stably expressing H3.1-SNAP and GFP-XPC. White arrowheads indicate the irradiated areas. The boxplots show quantifications of red fluorescence loss in

irradiated areas at 15 min compared to before laser micro-irradiation (data from n cells scored in two independent experiments). Scale bars, 10 μ m.

Figure S2: Conservative redistribution of parental histones to the vicinity of UVC-damaged regions. Related to Figure 2.

(A) Experimental procedure for measuring parental histone loss and redistribution around the UVC damaged area based on photo-activation of a 20 μ m² patch of pre-existing H3.3-PA-GFP histones in the cell nucleus and micro-irradiation in the center of the fluorescent histone patch with a 266 nm UVC laser (damage induction) or with a 488 nm bleaching laser (control). Fluorescence measurements are performed on 2D projections of 3D acquisitions in concentric regions around the site of laser micro-irradiation.

(B) Fluorescent patches of parental histones H3.3 (green) before and 15 min after local UVC damage (left) or local photo-bleaching (right) in U2OS cells stably expressing H3.3-PA-GFP and RFP-XPC. Green dotted lines delineate the cell nuclei. The edges of the fluorescent patches of parental histones before and 15 min after local irradiation are shown in white on the zoomed images.

(C) Quantification of the green fluorescence associated with parental H3.3-PA-GFP histones in concentric regions around the UVC damage site (purple) or the site of fluorescence bleaching with the 488 nm laser (green) at the indicated time points.

(D) Difference in green fluorescence distribution between the two time points obtained by subtracting 0 min from 15 min values quantified in (C). The position of the repair zone is based on RFP-XPC accumulation at 15 min. Error bars represent SD from n cells scored in two independent experiments.

(E) Fluorescent patches of parental histones H3.3 (red) before and 15 min after UVC laser micro-irradiation, followed by detergent extraction (Tx) in live U2OS cells stably expressing H3.3-SNAP and GFP. GFP solubilization is used as a control for Tx extraction. The graph displays quantification of red fluorescence distribution in concentric regions around the UVC damage site before (-Tx) and after detergent extraction (+Tx) as depicted on the scheme (data from n cells scored in two independent experiments). Scale bars, 10 μ m.

Figure S3: Parental histone redistribution is controlled by the repair factor DDB2. Related to Figure 3.

(A) Simplified scheme of the NER pathway showing the different repair factors that were targeted by siRNAs in this study. GG-NER: Global Genome NER, TC-NER: Transcription-Coupled NER.

(B, C) Distribution of parental histones H3.3 (red) 15 min after UVC laser micro-irradiation in U2OS cells stably expressing H3.3-SNAP and GFP-XPC treated with the indicated siRNAs

(siLUC: control). siRNA efficiencies were verified by immunofluorescence 30 min after UVC irradiation through a micropore filter or by western-blot. The black arrowhead indicates full-length ERCC6 and the empty arrowheads points to a splice variant.

(D) Distribution of parental histones H3.3 (red) 15 min after UVC laser micro-irradiation in U2OS cells stably expressing H3.3-SNAP and GFP-DDB2 treated with the proteasome inhibitor MG132 or DMSO (vehicle). The efficiency of MG132 treatment was verified by immunoblot against ubiquitin (Ub). White arrowheads indicate the irradiated areas. Scale bars, 10 μ m. The boxplots show quantifications of red fluorescence loss in irradiated areas at 15 min compared to before laser micro-irradiation (data from n cells scored in two independent experiments).

Figure S4: Recovery of parental histones coupled to repair progression. Related to Figure 5.

(A) Characterization by western blot of the U2OS cell line stably expressing H3.3-SNAP and CFP-XPC. e: epitope tag.

(B) Dynamics of parental histones H3.3 (red) at the indicated points after local damage with the UVC laser (white arrowheads) or local bleaching of the red fluorescence with a 555 nm laser (empty arrowheads) in U2OS cells stably expressing H3.3-SNAP and GFP-XPC. The graph shows quantification of red fluorescence recovery in illuminated areas. Cells that did not repair efficiently (based on GFP-XPC retention) were excluded from the analysis.

(C) Dynamics of parental histones H3.3 (green) at the indicated time points after local UVC damage (white arrowheads) in U2OS cells stably expressing H3.3-PA-GFP and RFP-XPC. The graph shows quantification of green fluorescence recovery in illuminated areas. Error bars on the graphs represent SD from n cells scored in two independent experiments. Scale bars, 10 μ m.

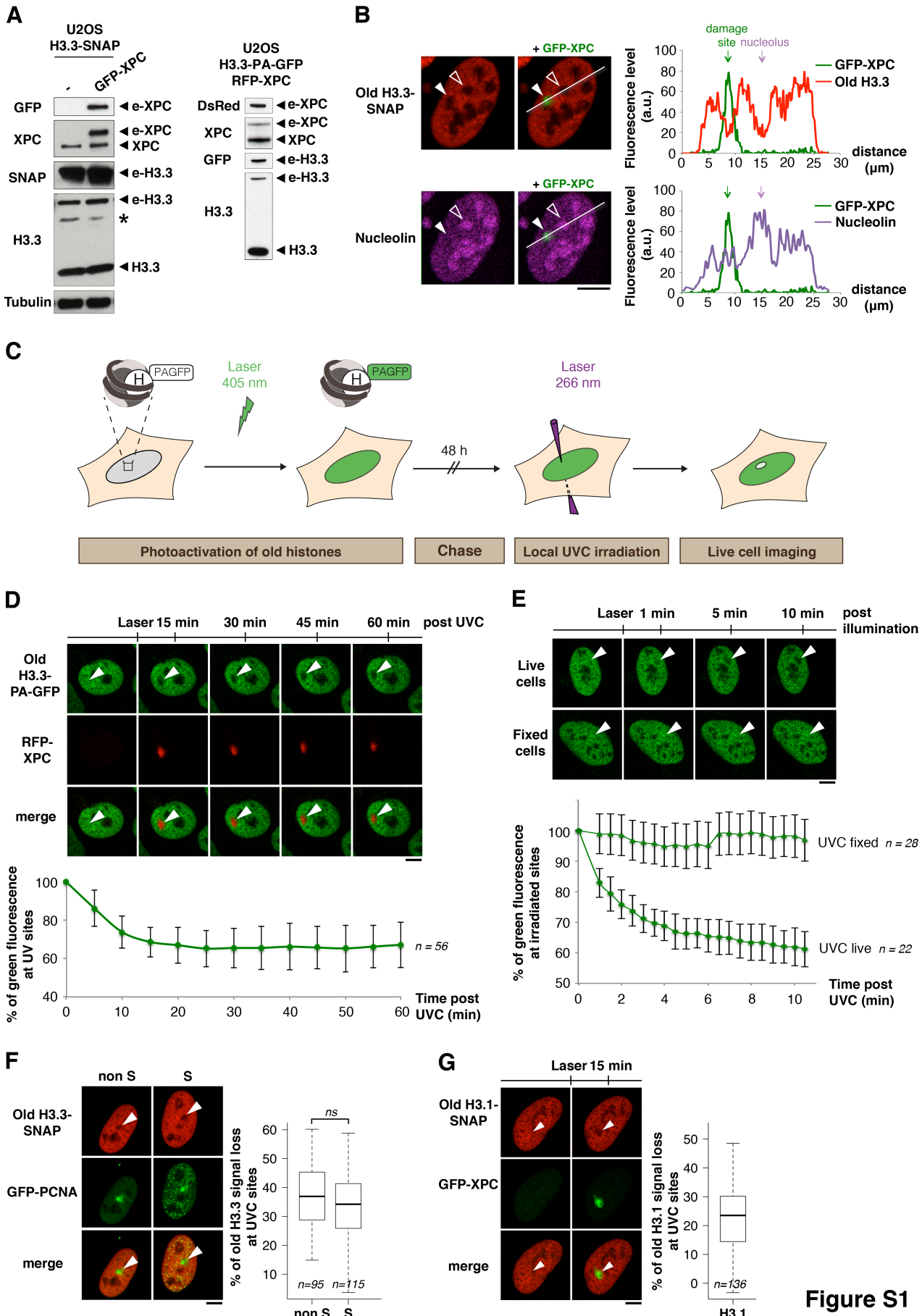
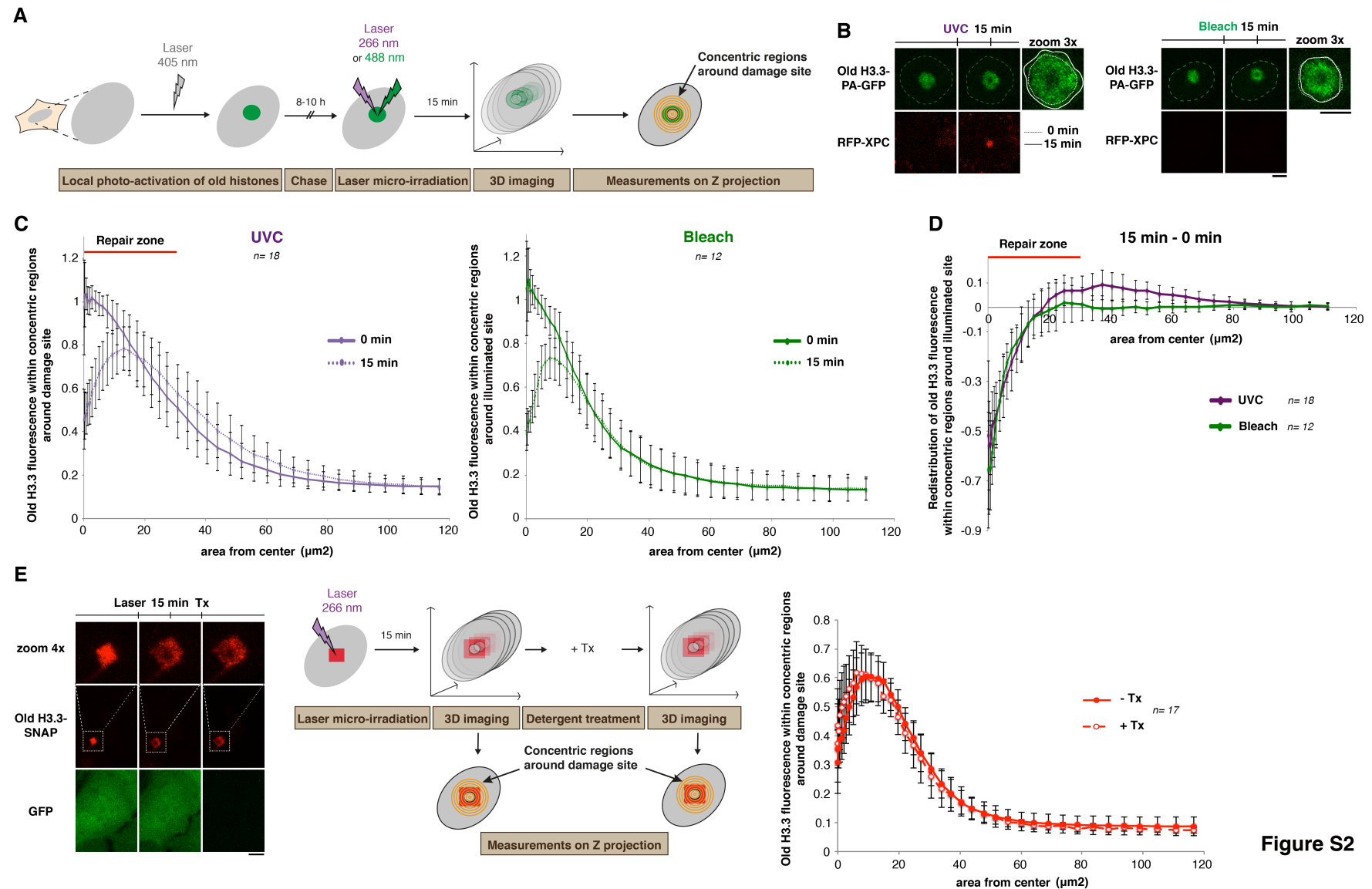


Figure S1



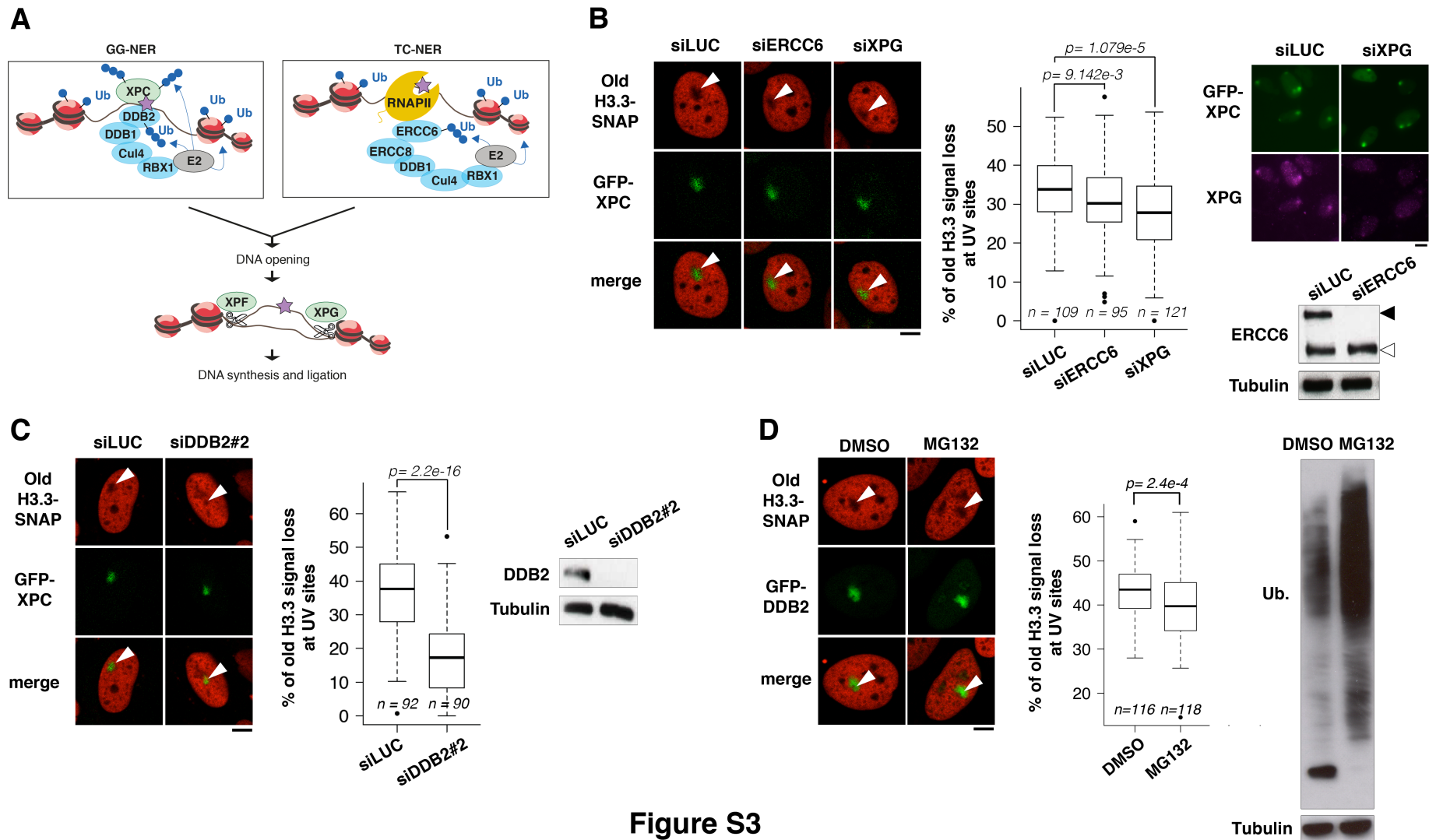


Figure S3

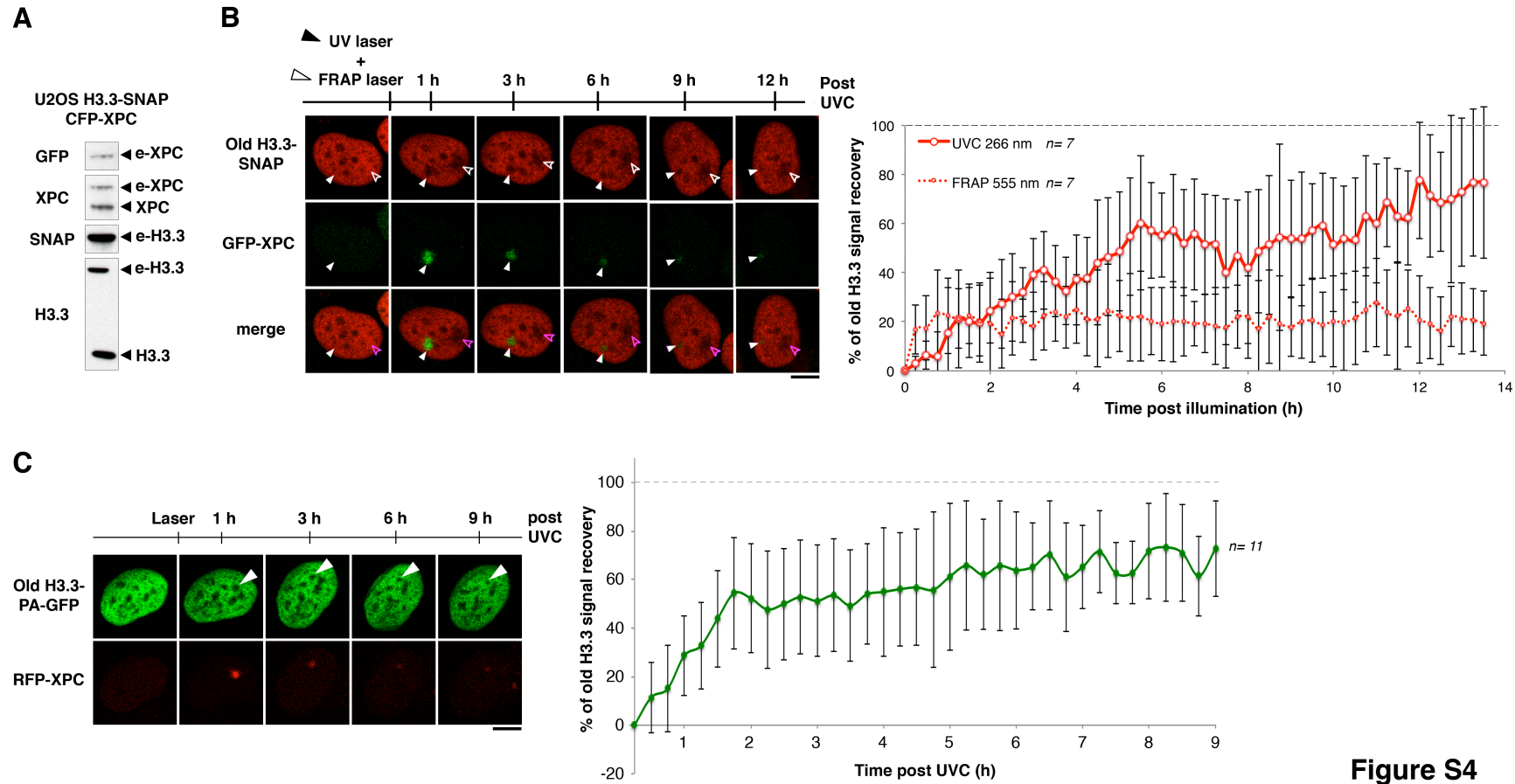


Figure S4